



A simulation study of hydraulic fracturing design in carbonate reservoirs: a middle east oilfield case study

Jing Yang¹ · Hui Liu¹ · Wei Xu¹ · Fang Liu¹ · Yanjun Fang² · Rongrong Jin¹ · Junjian Li²

Received: 1 April 2022 / Accepted: 22 October 2022 / Published online: 21 December 2022
© The Author(s) 2022

Abstract

The interactions between hydraulic fracture morphology and fluid transport mechanisms after large-scale fracturing in low-permeability carbonate reservoirs are important factors that could impact post-fracturing productivity. Using an integrated geology-engineering approach that consists of hydraulic fracturing and reservoir simulation, this paper presents the detailed hydraulic fracturing simulation and design of a low-permeability carbonate reservoir in the Middle East based on sweet spot mapping. The fracturing protocol is determined based on productivity charts, which are obtained via sweet spot mapping of the target carbonate reservoir. The daily production of a horizontal well in the reservoir shows an increase from 870 to 2000 bbl/d after the hydraulic fracturing design and implementation, which is the highest among the existing production wells in same oilfield. The results are shown to be consistent with the proposed productivity chart, which suggests that the implemented workflow could be helpful for the large-scale fracturing implementation of similar carbonate reservoirs.

Keywords Carbonate reservoir · Hydraulic fracturing design · Productivity chart · Sweet spot

Abbreviations

c	The empirical coefficient of compressive strength and tensile strength of rock
d	Correction coefficient, 1.2
E_d	Dynamic Young's modulus, GPa
G	Shear modulus, GPa
g	Acceleration of gravity, m/s ²
h	Formation depth, m
P_p	Reservoir pore pressure, MPa
P_f	Rupture pressure, MPa
P_p	Reservoir pore pressure, MPa
P_{frac_T}	Fracture toughness, MPa, here refers to type I fracture
S_t	Tensile strength, MPa
S_c	Compressive strength, MPa
V_{sh}	Mud content, decimal
Y	Young's modulus, psi

Greek

α	Biot elastic coefficient, decimal
β_1, β_2	Horizontal tectonic stress coefficient, decimal
$\rho_r(h)$	Overburden density with depth, kg/m ³
ν	Poisson's ratio
μ_d	Dynamic Poisson's ratio, decimal
σ_z	Vertical stress, MPa
σ_H	Maximum horizontal stress, MPa
σ_h	Minimum horizontal stress, MPa
σ_v	Vertical principal stress, MPa

Introduction

Due to the ultra-low porosity and permeability of low-permeability carbonate reservoirs, economic development cannot be achieved by conventional production methods, and large-scale fracturing treatments are shown to provide economic production (Zillur et al. 2002; Jeon et al. 2016; Qiao et al. 2022). For hydraulic fracture modeling, many simulation studies approximated the fractures as simple double-wing plane-like fractures and used local mesh refinement to simulate the stimulated volume after hydraulic fracturing (Zhao et al. 2022). In real applications, the fracture networks formed after large-scale fracturing of horizontal wells are rather complex, these simplified and approximate methods are insufficient to simulate production behavior from the real fracture networks after hydraulic fracturing.

✉ Junjian Li
junjian@126.com

¹ Research Institute of Petroleum Exploration and Development, China National Petroleum Corporation, Beijing 100083, China

² State Key Laboratory of Petroleum Resources and Prospecting, China University of Petroleum, Beijing 102249, China

The geological, geomechanical, and development factors that affect the geometry of the hydraulic fracture network include the value and orientation of in-situ stress, the properties of natural fractures such as distributions and densities, fracturing design and implementation, as well as pumping parameters (Cipolla et al. 2011a and 2011b; Sun et al. 2015; Vishkai and Gates, 2019; Suboyin et al. 2020). The integrated geological engineering technology, which is based on the coupled simulation of fracture propagation and reservoir fluid flow, has been shown to be an effective tool that can comprehensively consider the influence of above factors (Olsen 2008; Cheng et al. 2012; Weng et al. 2014; Wu and Olson, 2015; Wu et al. 2015; Zhang et al. 2020; Fu et al. 2020).

At present, many papers have present field applications using the integrated geologic and engineering approach for hydraulic fracturing modeling and production forecast in unconventional oil and gas reservoirs, but mainly for tight sandstone and shale formations (Wu et al. 2015; Saberhosseini et al. 2017; Vishkai and Gates 2019; Wang et al. 2019; Yong et al. 2021; Lu et al. 2022a and 2022b). In this paper, this method is applied to the hydraulic fracturing design for a carbonate reservoir in Middle East. Using the integrated geological engineering technology, an integrated workflow that couples fracturing modeling and reservoir simulation has been employed, from which the rock mechanics model and reservoir model have been calibrated via history matching against production data and pumping pressure history. Based on the calibrated models, physical sweet spots and engineering sweet spots are obtained, which represent the productivity of oil wells and the difficulty of hydraulic fracturing, respectively. As last, we show the hydraulic fracturing design and results for a horizontal well based on the productivity charts obtained via sweet spot mapping.

Background

The target reservoir is a typical low permeability and porosity carbonate reservoir in Iraq, and its reserves account for 24.9% of the whole oilfield. The vertical pay zone is divided into B1, B2, B3, and T layers, The B1 and B2 layers are mainly biochip pores, and the average pore throat radius is about 0.1 μm , which is microporous media. The average porosity of B1 and B2 layers is 15.5–17.6%, and the permeability is lower than 0.1mD. The porosity and permeability of B3 and T layers are slightly higher, but the proportion of reserves is low (<30%).

There are three hydraulically fractured wells (H5S, N55, and N52) in the target reservoir, among which the H5S well has the best performance after fracturing and the N52 well

has the worst performance, as shown in Fig. 1. Fig. 1 Daily oil production of three hydraulically fractured wells 1.

The production of fractured wells is not only affected by fracturing scale, well type, horizontal length, numbers of fracturing stages, but also affected by reservoir petrophysical parameters and rock mechanics parameters. Therefore, it is important to analyze the main controlling factors of productivity to determine the optimum well location and fracturing scale.

An integrated workflow of hydraulic fracturing modeling

The integrated workflow consists of the following steps as shown in Fig. 2:

- (1) Set up one-dimensional and three-dimensional rock mechanics model using well-log data.
- (2) Fit and adjust the rock mechanics model by comparing against experimental data and pumping pressure history of fractured wells.
- (3) Determine the engineering sweet spots based on rock mechanic model and parameters; physical sweet spots are determined based on reservoir petrophysical data.
- (4) Implement the fracturing scheme for different sweet spot combinations and obtain the optimum fracturing parameters based on post-fracturing productivity and reservoir pressure distribution, as shown in Fig. 2. Fig. 2 the Integrated Workflow of hydraulic fracturing and reservoir modeling2

The detailed implementation of the integrated workflow described in Fig. 2 above consists of geological analysis, rock mechanics interpretation, fracturing modeling, and reservoir evaluation. Figure 3 below demonstrates the software used for these analyzing and modeling processes, which includes Techlog (for well logging analysis), Petrel

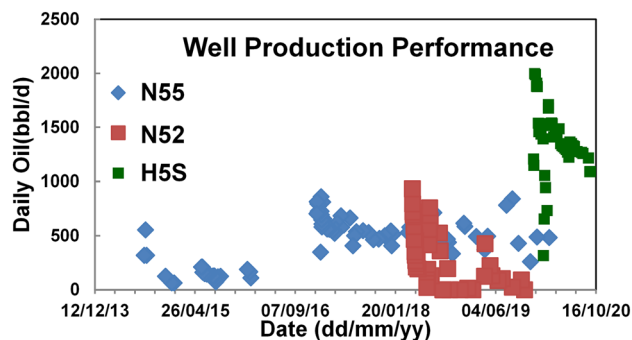


Fig. 1 Daily oil production of three hydraulically fractured wells 1

Fig. 2 the Integrated Workflow of hydraulic fracturing and reservoir modeling²

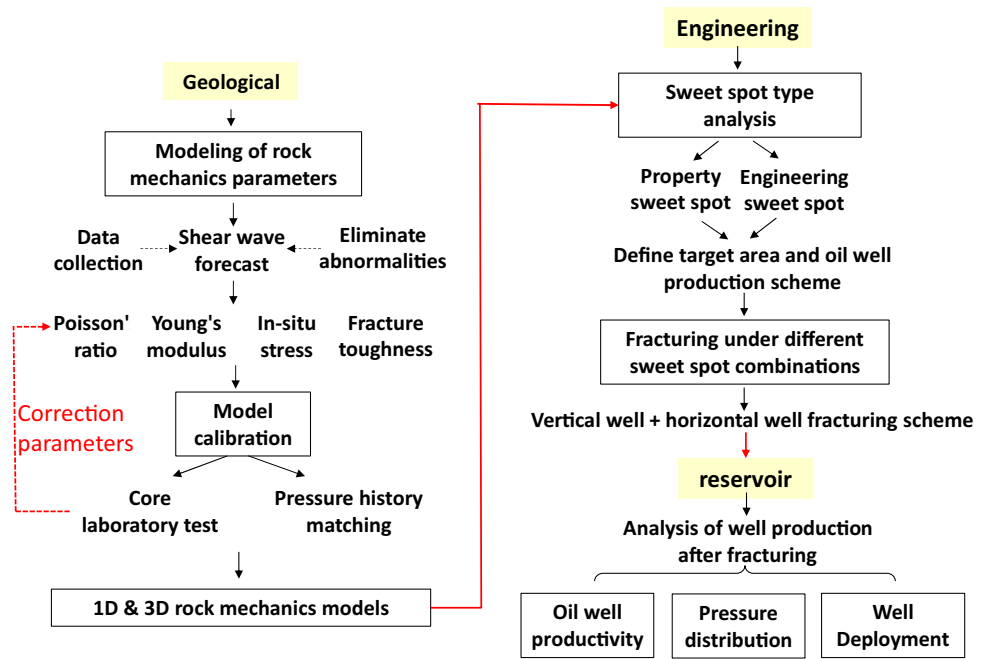
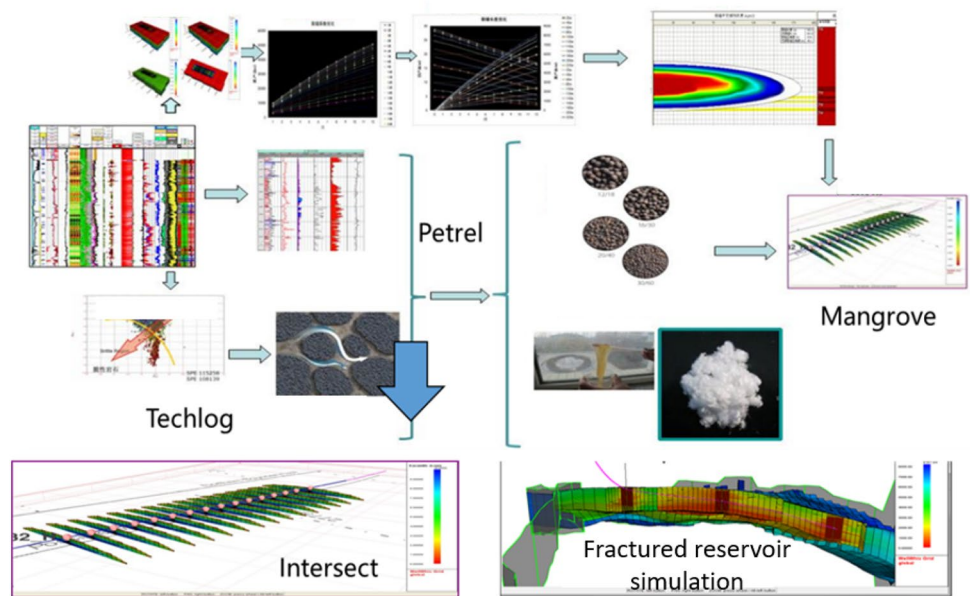


Fig. 3 Complete implementation diagram of the integrated process of geology, engineering, and reservoir simulation³



(for geological modeling), Mangrove (Kinetix), and Intersect (for fracturing modeling and reservoir simulation).

Geomechanics

As provided in Table 1 below, the data used for geomechanical modeling include P-wave time difference and natural gamma ray log curves of a total of 363 wells, laboratory experimental parameters (e.g. static and dynamic Young's modulus) of the one well (well V36), and fracturing

parameters of four hydraulically fractured wells, which can be used as the data set for rock mechanics model.

Shear wave prediction

There is a total of eight wells that have S-wave data that meet the requirements of rock mechanics calculation, which is insufficient for the rock mechanics model in the area. At present, most shear wave prediction methods use empirical formula. Which does not consider the characteristics of the actual reservoir, nor does it consider the influence

Table 1 Data sources of reservoir geomechanical model construction1

The data source	Parameter	Purpose
363 wells	P-wave time difference, natural gamma ray, clay content, physical properties interpretation results from well logging	Calculate the one-dimensional rock mechanics parameters
One well (V36)	Static and dynamic young's modulus, Poisson's ratio, magnitude and direction of in-situ stress, compressive/tensile strength, and other laboratory experimental parameters	Calibrate one-dimensional rock mechanics parameter calculation results to ensure the reliability of parameter calculation
Existing 4 fractured wells	in-situ stress, and fracture height obtained from pumping pressure history matching	Adjust rock mechanics parameters

of different formation properties on the prediction of shear wave time difference. Therefore, rock mechanics calculation based on shear wave prediction obtained by empirical method tends to lead to unreasonable subsequent parameters (Al-Ruwaili and Chardac, 2003). This study fully considers the geological characteristics, takes the wells with S-wave as the template, and predicts the S-wave data of other wells through a multi-factor neural network. The procedure is as follows:

(1) The influencing factor set

Three indexes, including compressional wave, gamma ray, and shale content, are used as the influencing factor set for a single well.

(2) Multi-well training

Based on all the wells with the complete data set of shear wave, compressional wave, gamma ray, and shale content, data training is conducted to establish the nonlinear relationship between compressional wave, gamma ray, shale content, and shear wave to prepare for the next fitting test.

(3) Fitting existing well S-wave data

To establish the relationship between multiple indicators and S-wave time difference, the existing S-wave data of the wells are fitted, and the parameters of the constructed neural network are adjusted to obtain the S-wave data predicted by the model match the actual S-wave data. The resulting neural network model is used to predict the S-wave data of other wells.

(4) Prediction of shear wave data of unknown Wells

The fitted neural network model is used to predict shear wave data of other wells. Taking compressional wave, gamma ray, and shale content of other wells as input data, the S-wave data of this well is obtained through the calculation of the existing neural network model.

See Fig. 4 for the schematic diagram of the above process. Detailed calculation results are shown in Fig. 5.

The comparison between the measured and predicted S-wave data from eight wells is shown in Fig. 6. It can be

observed that the predicted results can take the variation characteristics of S-wave data are fully captured.

Rock mechanics parameters

Young's modulus and Poisson's ratio

In this study, dynamic Young's modulus and dynamic Poisson's ratio are obtained using the following correlation based on P-wave and S-wave data and are calibrated with measured data, as shown in Fig. 7.

$$E_d = 929 \cdot 10^5 \cdot \frac{\rho}{\Delta t_s^2} \cdot \frac{3\Delta t_s^2 - 4\Delta t_p^2}{\Delta t_s^2 - \Delta t_p^2} \quad (1)$$

$$\mu_d = \frac{0.5\Delta t_s^2 - \Delta t_p^2}{\Delta t_s^2 - \Delta t_p^2} \quad (2)$$

where

E_d — Dynamic Young's modulus, GPa;

μ_d — Dynamic Poisson's ratio, decimal.

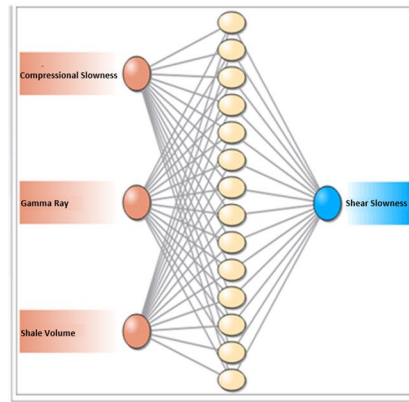
The acoustic logging curve is used to calculate the young's modulus and Poisson's ratio, which are dynamic values. They need to be converted to static ones for simulation after combing with the experimental data via regression. In Fig. 8, static data are from triaxial stress test results, and dynamic data are from acoustic characteristics test results.

According to the static and dynamic conversion relationship between Young's modulus and Poisson's ratio in Fig. 8, the parameters measured in the front acoustic logging are converted to obtain the static parameters, which are compared with the triaxial stress static test results (taking well V36 as an example, as shown in Fig. 9). The errors of the two parameters are small and meet the requirements of rock mechanics parameter calculation.

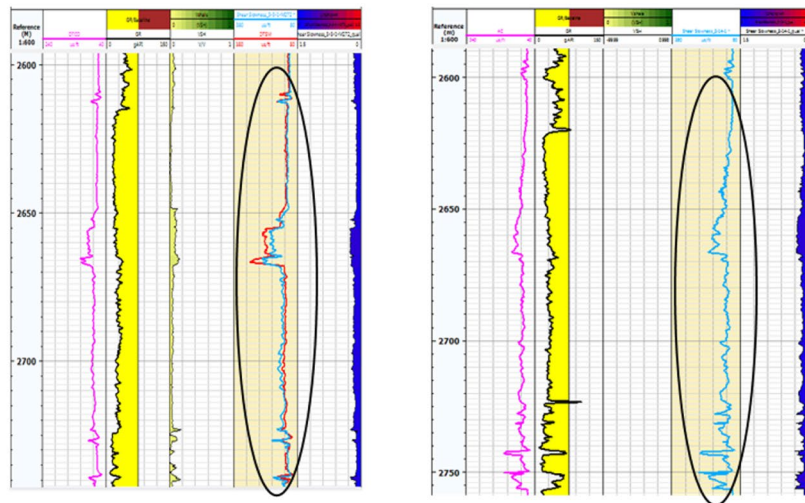
Other parameters

Based on the above calculation of rock mechanical parameters, the maximum horizontal principal stress, minimum

Fig. 4 Shear wave prediction based on a neural network model



a Constructing neural network model



b Fitting existing S-wave data

c Prediction of shear wave data for other wells

horizontal principal stress, fracture pressure, vertical stress, fracture toughness, shear modulus, confining pressure, pore pressure gradient, vertical stress gradient, and other indicators are also calculated. The corresponding calculation model is as follows:

Maximum horizontal principal stress (the calculation results are shown in SHMax in Fig. 10):

$$\sigma_H = \frac{\mu_s}{1 - \mu_s} (\sigma_v - \alpha P_p) + \beta_2 (\sigma_v - \alpha P_p) + \alpha P_p \quad (3)$$

Minimum horizontal principal stress (The calculation results are shown in SHMin in Fig. 10):

$$\sigma_h = \frac{\mu_s}{1 - \mu_s} (\sigma_v - \alpha P_p) + \beta_1 (\sigma_v - \alpha P_p) + \alpha P_p \quad (4)$$

Rupture pressure (The calculation results are shown in Pfrac in Fig. 10):

$$P_f = 3\sigma_h - \sigma_H - \alpha P_p + S_z \quad (5)$$

Tensile strength (The calculation results are shown in TSTR in Fig. 11):

$$S_t = S_c / c \quad (6)$$

The calculation formula of S_c :

$$S_c = (0.0045 E_D (1 - V_{sh}) + 0.008 E_D V_{sh}) \times 1000d \quad (7)$$

Vertical stress (The calculation results are shown in SHV in Fig. 11):

$$\sigma_z = 10^6 \int_0^H \rho_r(h) g dh \quad (8)$$

Fracture toughness (The calculation results are shown in Pt in Fig. 11):

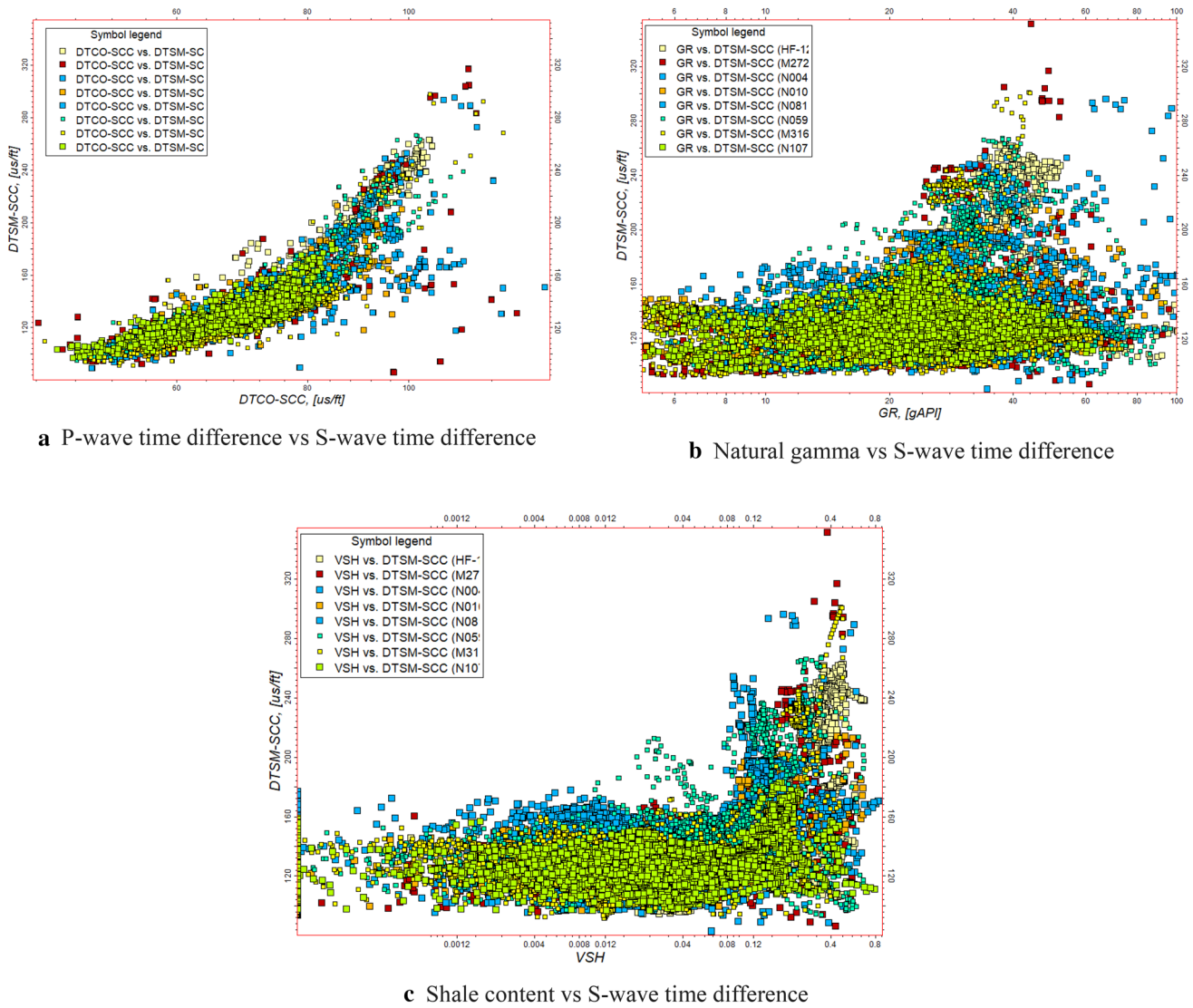


Fig. 5 Shear wave prediction calculation results based on a neural network model

$$P_{frac_T} = 0.217P_c + 0.0059S_t^3 + 0.0923S_t^2 + 0.517S_t - 0.3322 \tag{9}$$

Confining pressure (The calculation results are shown in P_c in Fig. 11):

$$P_c = \frac{\mu_s}{(1 - \mu_s)} (\sigma_z - \alpha P_p) + \alpha P_p \tag{10}$$

Shear modulus (The calculation results are shown in $YMOD$ in Fig. 11):

$$G = \frac{E_d}{2(1 + \mu_d)} \tag{11}$$

where,
 σ_H – Maximum horizontal stress, MPa;

σ_h – Minimum horizontal stress, MPa;
 σ_v – Vertical principal stress, MPa;
 P_p – Reservoir pore pressure, MPa;
 α – Biot elastic coefficient, decimal, theoretical value is "1-porosity", but needs to be adjusted in the fitting;
 β_1, β_2 – horizontal tectonic stress coefficient, decimal.
 P_f – Rupture pressure, MPa;
 P_p – Reservoir pore pressure, MPa;
 S_t – Tensile strength, MPa;
 c – The empirical coefficient of compressive strength and tensile strength of rock, the value is generally between 2–20;
 S_c – Compressive strength, MPa;
 V_{sh} – Mud content, decimal;
 d – Correction coefficient, 1.2;
 σ_z – Vertical stress, MPa;
 $\rho_r(h)$ – Overburden density with depth, kg/m^3 ;

Fig. 6 Comparison between measured and predicted shear wave data

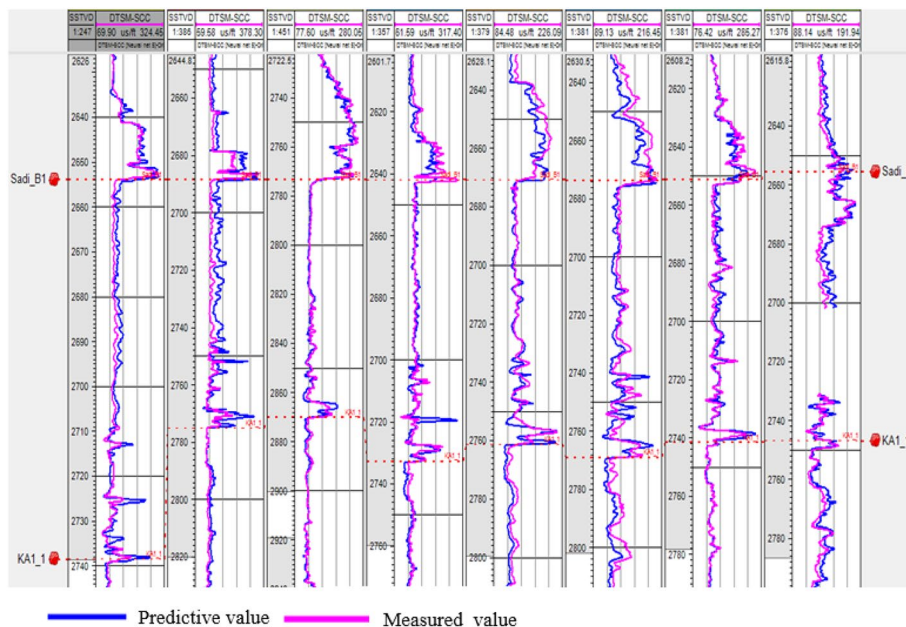
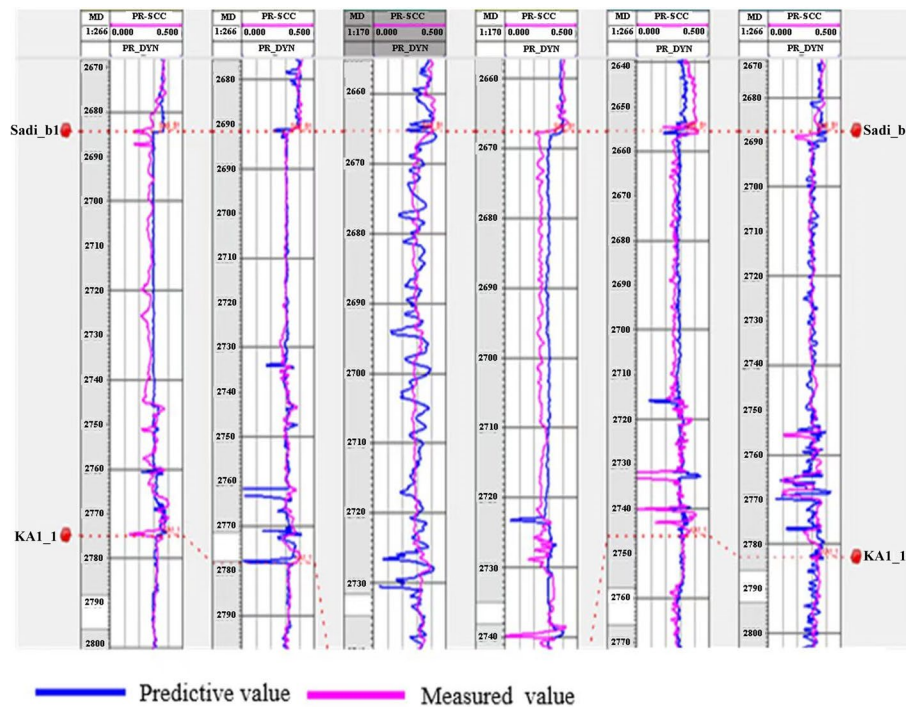


Fig. 7 Comparison between calculated and measured dynamic Poisson's ratio



h – Formation depth, m;
 g – Acceleration of gravity, m/s^2 ;
 P_{frac_T} – Fracture toughness, MPa, here refers to type I fracture;
 G – Shear modulus, GPa;

1D and 3d rock mechanics models

Based on the above geomechanical model and typical mechanical parameter calculation model, one-dimensional

rock mechanical parameters of more than 300 wells are predicted in combination with the location of the drilling platform. For the target area, two existing fractured Wells N52 and H5S are taken as examples, as shown in Figs. 11 and 12.

Based on the one-dimensional rock mechanics model, the arithmetical average method is used to discretize the predicted rock mechanics parameters longitudinally. Young's modulus, Poisson's ratio, and horizontal principal stress are taken as examples, as shown in Figs. 12, 13, and 14.

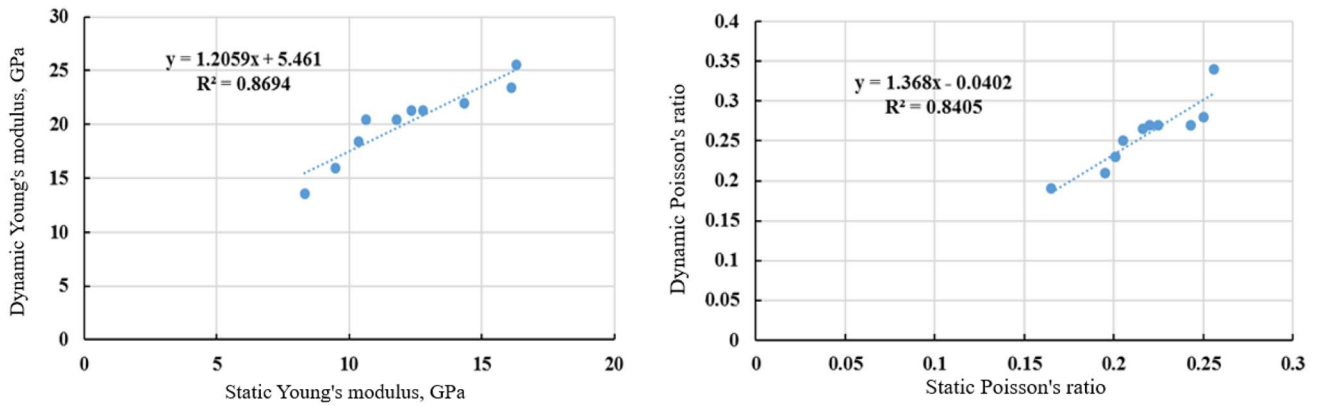


Fig. 8 Calculation results of Dynamic Young's modulus and Poisson's ratio in well V36

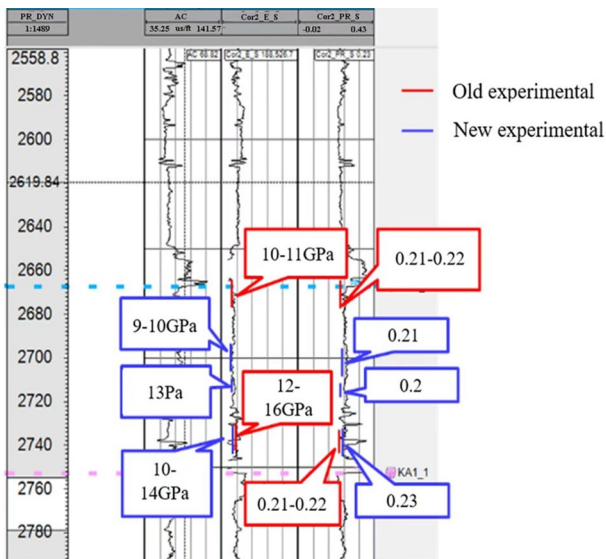


Fig. 9 Comparison of calculation results of static Young's modulus and Poisson's ratio with experimental static data in well V36

Furthermore, 3D rock mechanics model is obtained through plane prediction. Due to the uncertainties in the geological model, geomechanical model, and fracture propagation simulation model, further calibration and correction of input parameters are needed to ensure the accuracy of simulation results. The comprehensive calibration flow chart is shown in Fig. 15. The correction results are shown in Figs. 16, 17, and 18.

Sweet spot mapping

(1) Engineering sweet spots

Considering the characteristics of reservoir rocks in interest, we focus on the brittleness index, horizontal principal stress and fracture toughness, which is used to

set up the fracturing index, namely engineering sweet spots, representing the level of easiness of fracturing. The index is further divided into three levels: I, II, and III, of which level I reservoir quality represents the easiest cases of fracturing. The classification of engineering sweet spots is summarized in Table 2.

(2) Physical sweet spots

In this study, petrophysical properties such as permeability, porosity, oil saturation, and effective thickness are considered to characterize the capability of post-fracturing oil production. Like the engineering sweet spots, the physical sweet spot index is divided into three levels, of which level I reservoir is the best, representing the highest oil production capability. The classification of engineering sweet spots is summarized in Table 3.

Based on the classification of engineering and physical sweet spots indexes, the sweet spot maps are obtained respectively, as shown in Fig. 19 and Fig. 20. There are engineering sweet spots in the middle and southeast of B1 and B2 layers, but there are few engineering sweet spots in the middle of B3 layers, and there are no engineering sweet spots in T layers. B1 and B2 layers are the main layers for hydraulic fracturing deployment, given the physical sweet spot distribution. In the middle of B2 layer, physical sweet spots are developed, while in B1 layer, physical sweet spots of B3 and T are the least developed. Considering the relatively high permeability in B3 and T layers, hydraulic fracturing is not recommended in B3 and T layers.

Productivity evaluation when fracturing under different sweet spot combinations

This section takes B2 layer as example and provides the post-fracturing productivity forecast for the wells under different hydraulic fracturing parameters. Based on the

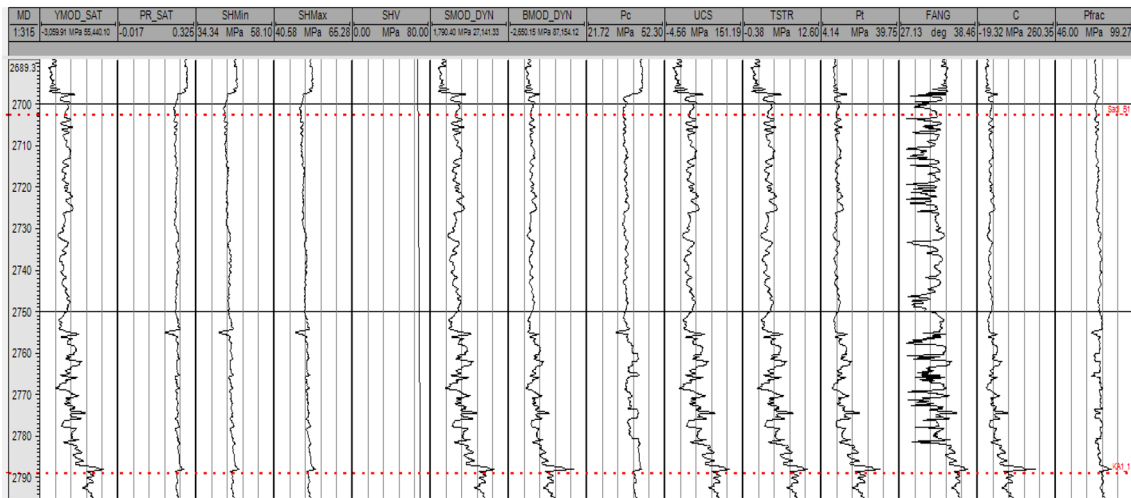


Fig. 10 One-dimensional rock mechanics parameters of well H5S

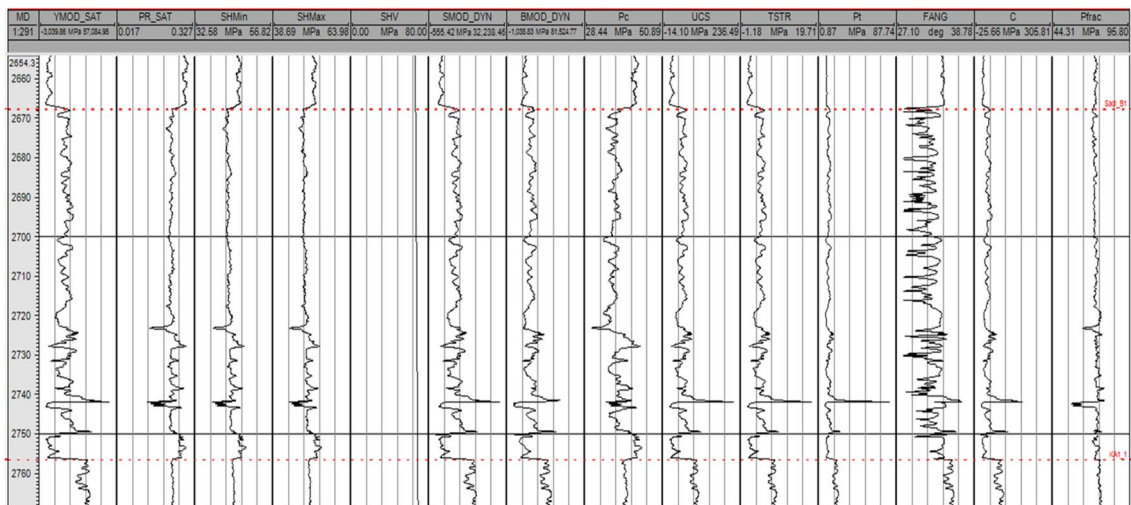


Fig. 11 One-dimensional rock mechanics parameters of well N52

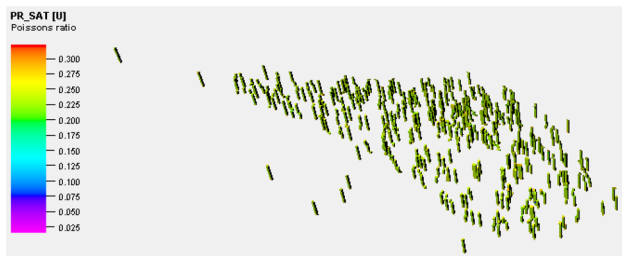


Fig. 12 Longitudinal discretization of Poisson's ratio

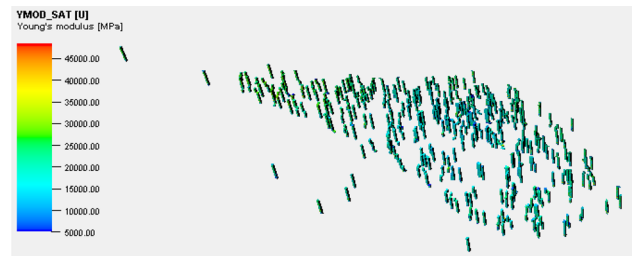


Fig. 13 Longitudinal discretization of Young's modulus

combination of sweet spots, B2 layer can be divided into the following sweet spot combinations as shown in Table 4. The sweet spots of Physical 1 + Engineering 1, Physical

2 + Engineering 1 and Physical 3 + Engineering 1 are the main ones, which account for 42.74% of reserves, and thus are studied in detail here.

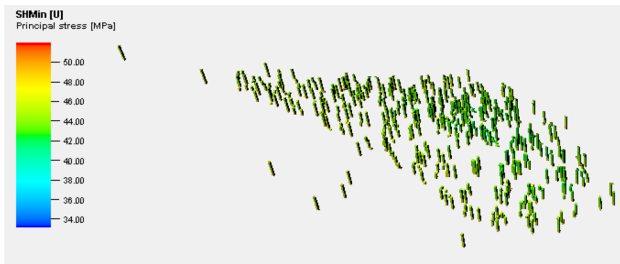


Fig. 14 Longitudinal discretization of minimum horizontal principal stress

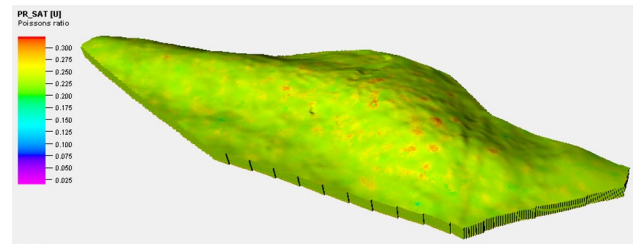


Fig. 16 Poisson's ratio

To evaluate the single well production capability under different sweet spot combinations, the volume of the proppant and fracturing fluid, number of fracturing stages, and horizontal section length are considered as control variables, based on which six different fracturing schemes are proposed. We further discuss the effects of changing these variables on horizontal good productivity.

Three combinations of Physical 1 + Engineering 1, Physical 2 + Engineering 1, and Physical 3 + Engineering 1 are analyzed. The fracture half-length obtained by fracturing simulation is mainly between 75-135 m, and the conductivity is mainly between 1200-2100mD.m. In the fracturing process of horizontal wells, fracture distribution under different proppant amount is illustrated in Fig. 21. Compared to using 50000 kg proppant, when the amount of proppant is 150000 kg, fracture length is higher and fracture volume is larger, which leads to higher productivity.

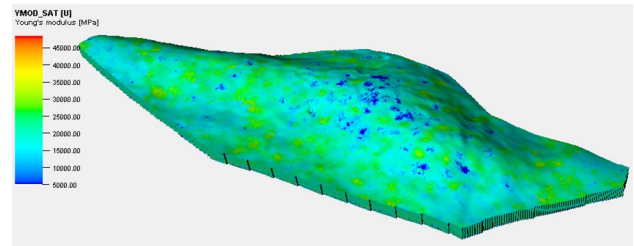
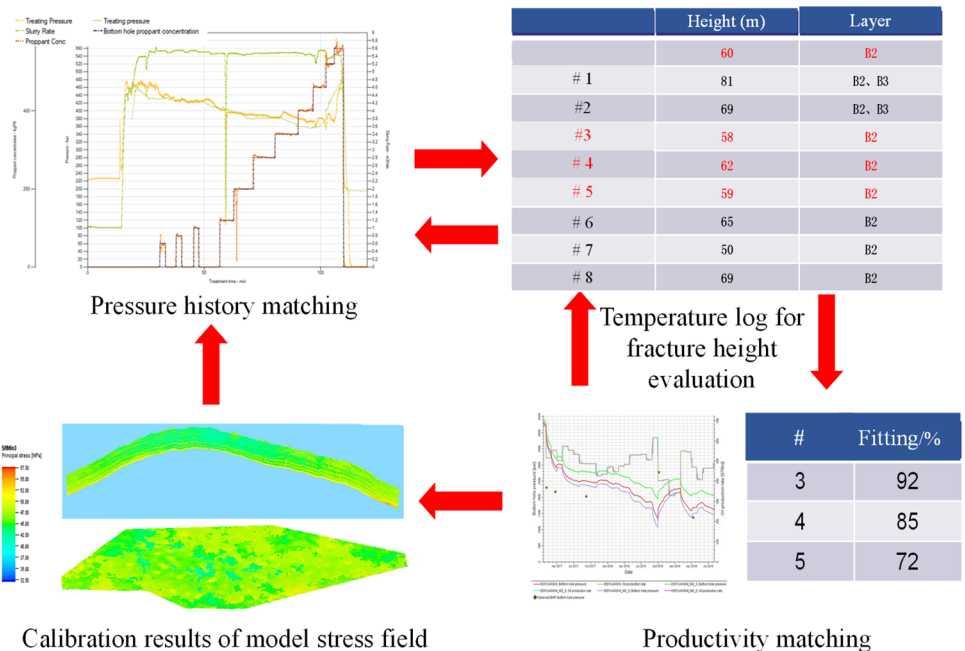


Fig. 17 Young's modulus

For the combination of Physical 1 + Engineering 1, the productivity of each scheme is shown in Fig. 22 below.

As shown in Fig. 22, when the injected proppant ranges from 50,000 to 150,000 kg, the corresponding horizontal well productivity ranges from 1000 to 1600 bbl/d. When it comes to less than 900,00 kg, the amount of proppant injected has a strong effect on single well productivity. When the production per well reaches 1500 bbl/d at 90,000 kg of proppant, the rate increase with proppant amount becomes

Fig. 15 Comprehensive flow chart of the model calibration



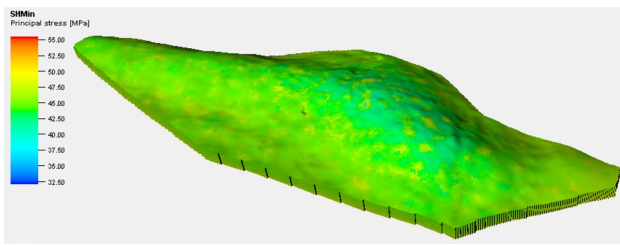


Fig. 18 Minimum horizontal principal stress

Table 2 Classification summary of single index of engineering sweet spots2

Level	Engineering sweet spots index		
	Brittleness index, %	Minimum horizontal stress /MPa	Fracture toughness/ Mpa.m ^{-0.5}
I	> 45	The < 42	The < 12
II	37 to 45	42–47	12–17
III	< 37	> 47	> 18

Table 3 Classification summary of single index of physical sweet spots3

Level	Physical sweet spots index			
	Permeability, mD	Porosity, %	Oil saturation, %	Effective thickness, m
I	> 1	> 20	> 65	> 20
II	0.051	10–20	40–65	10–20
III	< 0.05	< 10	< 40	< 10

less significant. The effect of fracturing fluid volume on single well productivity is smaller, as the fracturing fluid is between 400 m³ to 900 m³, the corresponding horizontal well productivity is 1400 to 1550 bbl/d. When fracturing fluid volume is less than 500/m³, the effect of increasing fracturing fluid volume on single well productivity becomes more significant. When the productivity of a single well is 1500 bbl/d, the effect of increasing fracturing fluid quality on single well productivity is weakened. The number of fracture stages and horizontal well sections have a significant effect on single well productivity when the production is observed to range from 1050 to 1600 bbl/d at 6 to 16 fracture stages. When the number of stages reaches 14, the increase in productivity is more obvious with the increasing number of stages, and then the effect becomes smaller. The horizontal section length has the greatest impact on productivity. When the horizontal section length is increased from 1000 to 2000 m, the productivity increases from 1500 to 2500

bbl/d. When the horizontal section length increases from 1000 to 1600 m, the effect is the most significant, and then the impact becomes less pronounced.

Based on the discussion above, for the sweet spot combination of Physical 1 + Engineering 1, proppant and horizontal length have a greater impact on productivity, while fluid volume has a smaller impact. The productivity chart of the sweet spot combination of Physical 1 + Engineering 1 is obtained, as shown in Fig. 23.

Through a similar analysis of Physical 1 + Engineering 1, the productivity charts of the combination of two sweet spots of Physical 2 + Engineering 1 and Physical 3 + Engineering 1 are obtained, as shown in Figs. 24 and Fig. 25.

By changing the four factors affecting the productivity of horizontal wells, the productivity range of each sweet spots combination horizontal well is obtained as follows:

Discussion

Through the productivity analysis of different sweet spot combinations in Sect. 4, the following understandings are obtained:

- (1) Based on the analysis of physical properties and distribution of engineering sweet spots, it can be observed that B1 and B2 layers have more engineering sweet spots in the middle and southeast, B3 layers have less engineering sweet spots in the middle, and T layers have no engineering sweet spots. B1 and B2 layers are the main layers for hydraulic fracturing. In the middle of B2 layer, physical sweet spots are developed. B2 layer is the main layer contributing to oil production. Considering that B3 and T layers have good permeability, production and development could be carried out without fracturing.
- (2) The sweet spot combination of Physical 3 + Engineering 1 yields the lowest production, ranging from 180 to 430 bbl/d. Physical 2 + Engineering 1 sweet spot combination yields high productivity, ranging from 500 to 1900 bbl/d; Physical 1 + Engineering 1 sweet spot combination leads to the highest capacity, ranging from 1000 bbl/d to 2500 bbl/d. For the sweet combination of physical 2 + Engineering 1 and physical 1 + Engineering 1, the productivity crossover part shown in Fig. 26 is mainly realized by increasing the length of horizontal section.
- (3) Under different sweet spot combinations, the productivity of sweet spots with different physical properties intersects with each other. The effect of level II and III physical sweet spots can be improved by taking the advantages of engineering sweet spots. Therefore, the sweet spot combination areas of Physical 1 + Engineer-

Fig. 19 Distribution of engineering sweet spots

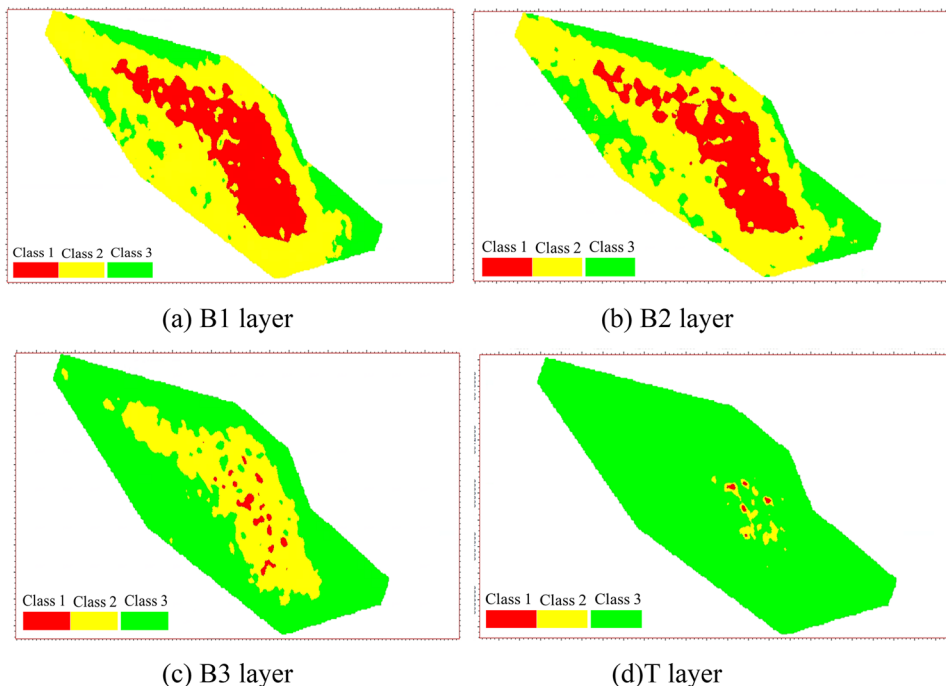


Fig. 20 Distribution of physical sweet spots

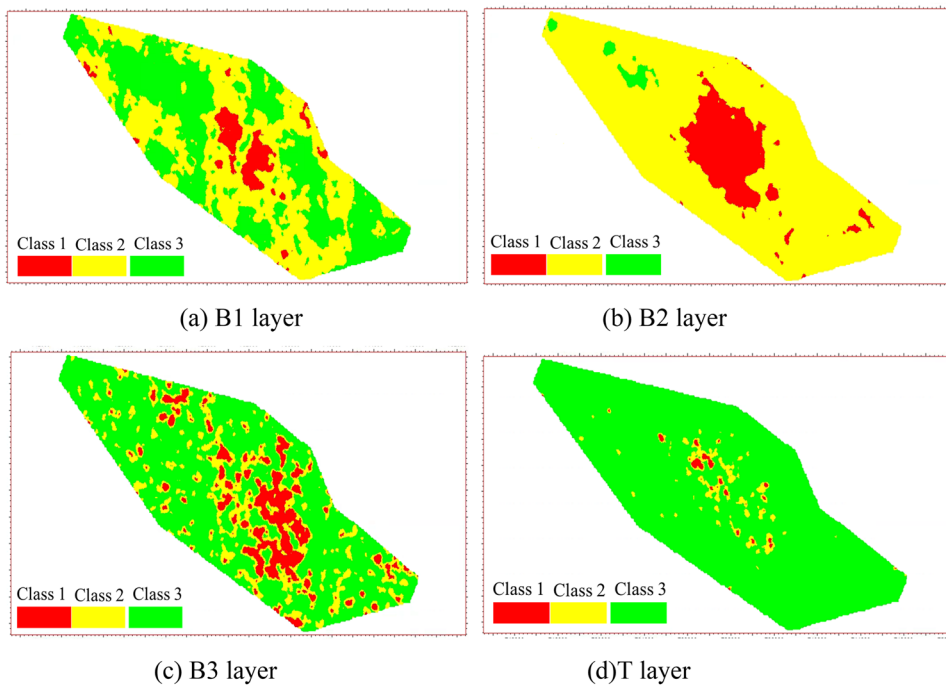


Table 4 Proportion of sweet spot combination in B2 layer

	Physical 1	Physical 2	Physical 3
Engineering 1	12.46%	19.72%	22.39%
Engineering 2	5.67%	9.02%	6.43%
Engineering 3	2.7%	9.95%	11.67%

ing 1 and Physical 2 + Engineering 1 should be considered as the main areas in the development process, while the sweet spot combination areas of Physical 3 + Engineering 1 should be ignored, and the model could further established to optimize the development

Fig. 21 Fracture under different proppant amount

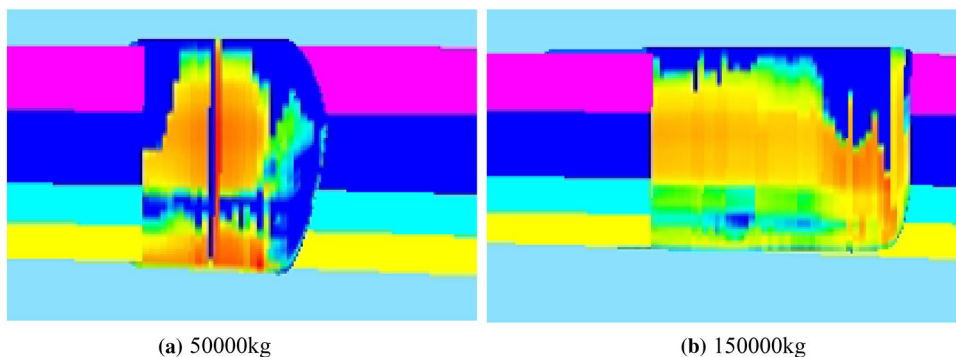
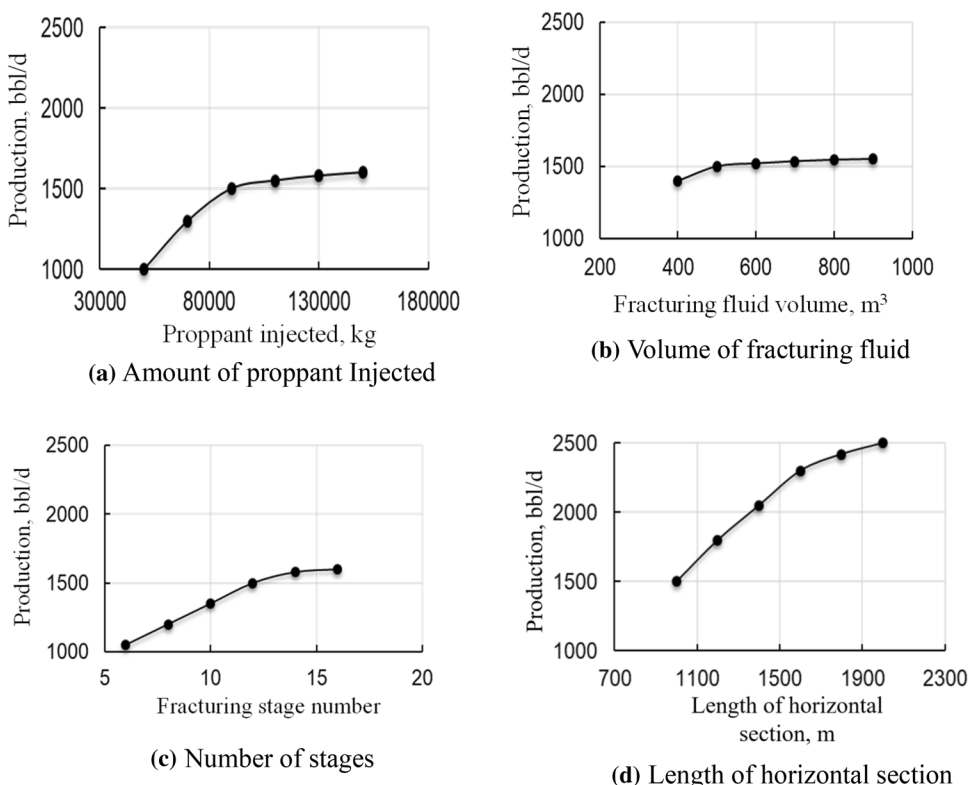


Fig. 22 Productivity changes under various factors



strategy by increasing the horizontal section length and proppant amount injected.

Application example

Here we show a preliminary application example, which is performed under the guidance of our observation above. Well H24S was put into production in December 2020, which is located in the combination area of physical sweet spot 1 + engineering sweet spot 1. It is perforated in B2 layer with a horizontal section length of 1000 m and 12 fracturing stages with an average fracturing fluid consumption of 500 m³ per stage. The initial fracturing production reaches above 2000 bbl/d and the production data show a relatively

extensive stabilized period of three months before declining, which suggests a satisfactory fracturing outcome as shown in Fig. 27. It can also be observed in Fig. 27 that the production of well H24S is consistent with the productivity chart.

Conclusions

This paper presents a field case study of hydraulic fracturing design of a low-permeability carbonate reservoir. Using the integrated geological and engineering modeling approach, the productivity charts based on physical and engineering sweet spots are constructed, and the following conclusions and understandings are obtained:

Fig. 23 Production capacity chart under various factors combination

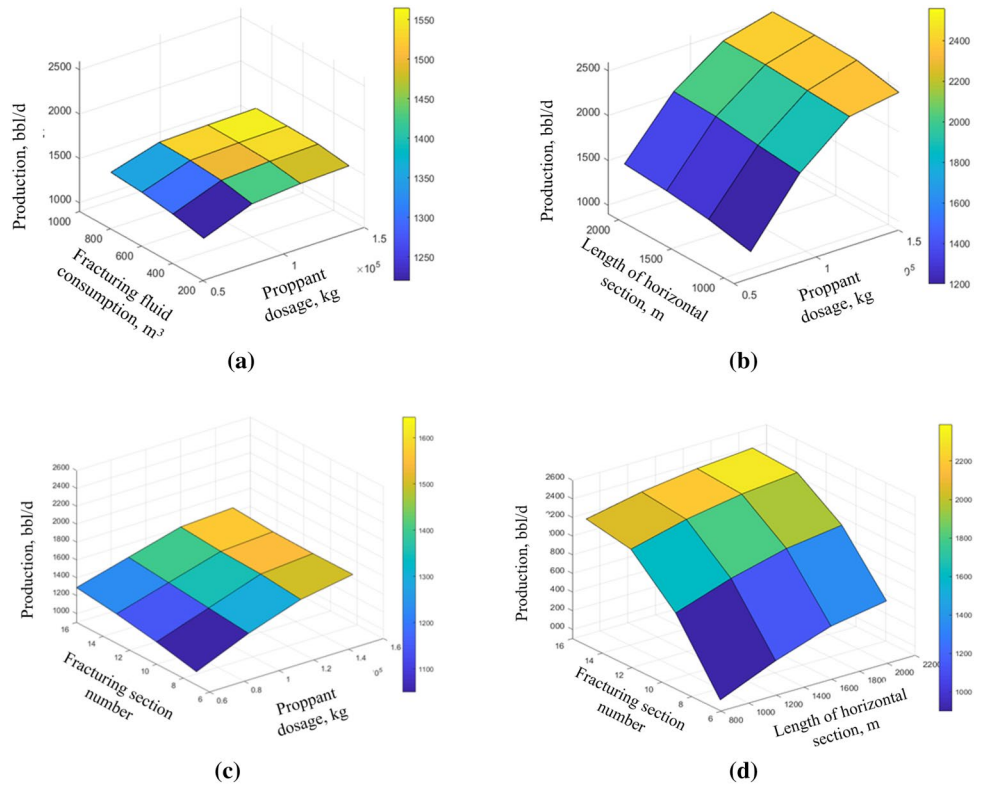


Fig. 24 Physical 2 + Engineering 1 capacity chart

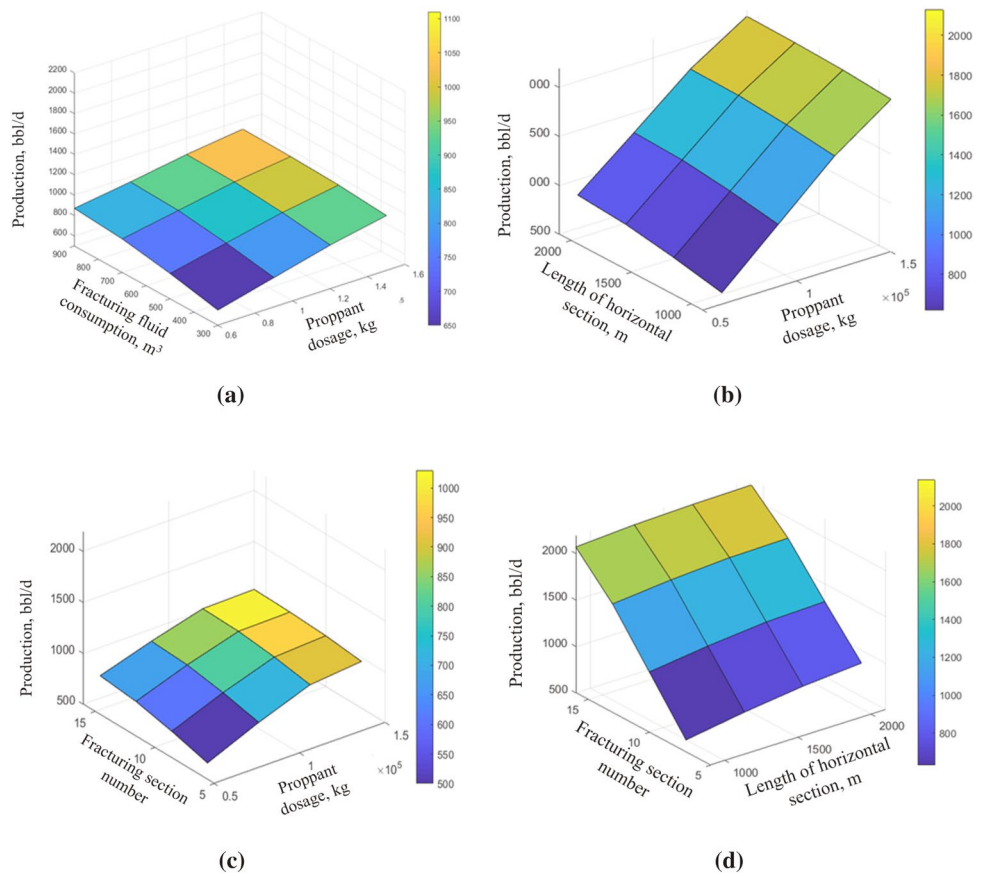


Fig. 25 Production capacity chart under various influencing factors

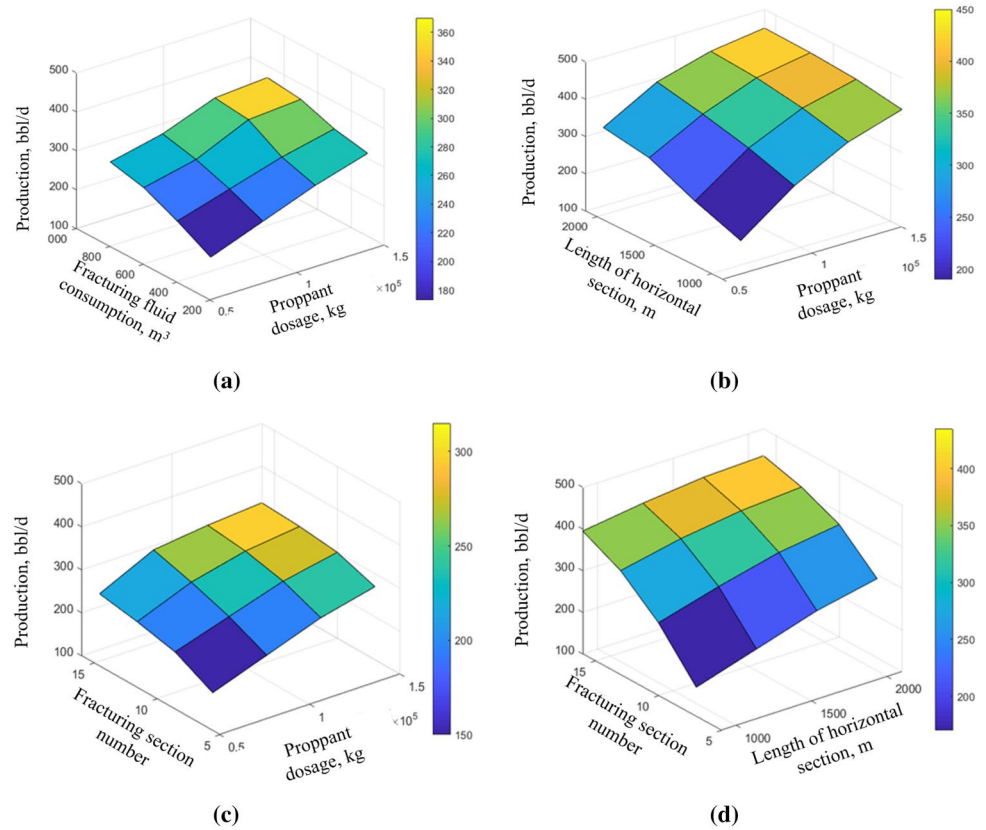
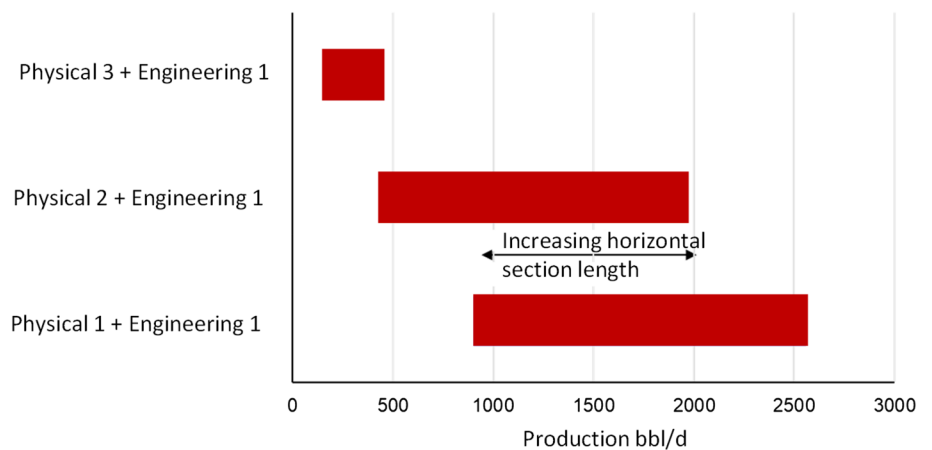


Fig. 26 Production range of different sweet spot combinations



- (1) The amount of proppant has a significant influence on fracture length and conductivity; thus the optimal proppant amount is the primary consideration in fracturing design.
- (2) The main controlling factors of the production capacity of wells with both good engineering sweet spot and good physical sweet spot are proppant amount and horizontal length. For the wells with good engineering sweet spot and middle physical sweet spot, the main controlling factors of the production capacity are proppant amount and horizontal well length; For the wells with good engineering sweet spot and poor physical properties, the main controlling factors of productivity are number of fracturing stages and horizontal length.
- (3) The productivity of wells with good engineering sweet spot and middle physical sweet spot can be improved through large fracturing scale. The hydraulic fracturing for wells with good engineering sweet spot and poor physical sweet spot could be excluded future fracture design due to low production capacity.
- (4) This study focuses on the effect of combination of physical and engineering sweet spots on the production capacity in the sweet spot mapping process. The influence of geomechanics models/ parameters variations on

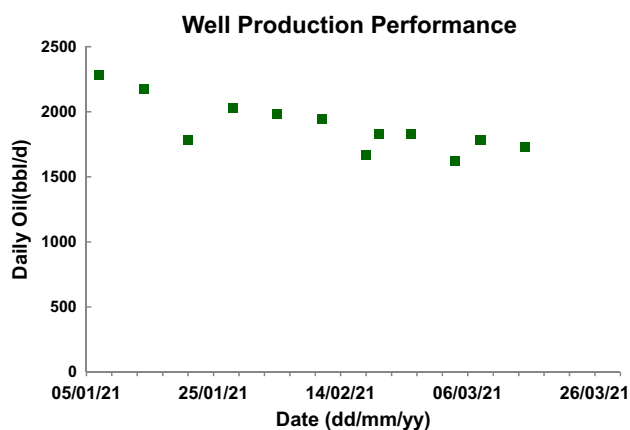


Fig. 27 Daily oil distribution of well H24S

fractures and production will be further studied in our future work.

Acknowledgments The authors would like to thank Schlumberger for providing software: Petrel, Visage, Kinetix, and Intersect for completing this study.

Declarations

Conflict of interest The authors declare no conflict of interest.

Open Access This article is licensed under a Creative Commons Attribution 4.0 International License, which permits use, sharing, adaptation, distribution and reproduction in any medium or format, as long as you give appropriate credit to the original author(s) and the source, provide a link to the Creative Commons licence, and indicate if changes were made. The images or other third party material in this article are included in the article's Creative Commons licence, unless indicated otherwise in a credit line to the material. If material is not included in the article's Creative Commons licence and your intended use is not permitted by statutory regulation or exceeds the permitted use, you will need to obtain permission directly from the copyright holder. To view a copy of this licence, visit <http://creativecommons.org/licenses/by/4.0/>.

References

- Suboyin A, Rahman MM, Haroun M. (2020) Hydraulic fracturing design considerations water management challenges and insights for Middle Eastern shale gas reservoirs. *Energy Reports* 6745–760 S2352484719308042. <https://doi.org/10.1016/j.egy.2020.03.017>
- Al-Ruwaili SB, Chardac O (2003) 3D model for rock strength and in-situ stresses in the Khuff formation of Ghawar field, methodologies and applications. Paper SPE-81476-MS presented at the Middle East Oil Show, Bahrain.
- Cheng Y (2012) Mechanical interaction of multiple fractures exploring impacts on selection of the spacing number of perforation clusters on horizontal shale gas wells. *SPE J* 17(04):992–1001
- Cipolla CL, Lewis RE, Maxwell SC, Mack MG (2011a) Appraising Unconventional resource plays: separating reservoir quality from completion effectiveness. Paper IPTC-14677-MS presented at the International Petroleum Technology Conference, Bangkok, Thailand.
- Fu S, Yu J, Zhang K, Liu H, Ma B, Su Y (2020) Investigation of multi-stage hydraulic fracture optimization design methods in horizontal shale oil wells in the Ordos Basin. *Geofluids* 2020:8818903
- Jeon J, Bashir MO, Liu J, and Wu X (2016) fracturing carbonate reservoirs: acidising fracturing or fracturing with proppants? Paper SPE-181821-MS presented at the SPE Asia Pacific Hydraulic Fracturing Conference, Beijing, China.
- Lu C, Jiang H, Yang J, Yang H, Cheng B, Zhang M, He J, Li J (2022a) Simulation and optimization of hydraulic fracturing in shale reservoirs: a case study in the Permian Lucaogou formation. *China, Energy Rep* 8:2558–2573
- Lu C, Jiang H, Yang J, Wang Z, Zhang M, Li J (2022b) Shale oil production prediction and fracturing optimization based on machine learning. *J Petrol Sci Eng* 217:110900
- Olson JE (2008) Multi-fracture propagation modeling: Applications to hydraulic fracturing in shales and tight gas sands. In *Proceedings of the 42nd US Rock Mechanics Symposium (USRMS)*, San Francisco, CA, USA.
- Qiao J, Tang X, Hu M, Rutqvist J, Liu Z (2022) The he hydraulic fracturing with multiple influencing factors in carbonate fracture-cavity reservoirs. *Comput Geotech* 147:104773
- Saberhosseini SE, Mohammadrezaei H, Saeidi O, Zadeh NS, Senobar A (2017) Optimization of the horizontal-well hydraulic-fracture geometry from caprock-integrity point of view using fully coupled 3D cohesive elements. *SPE Prod Oper* 33(02):251–268
- Sun Z, Liu C, Huang Z, Zhang R (2015) Mechanical Interaction of Multiple 3D Fractures Propagation for Network Fracturing. Paper SPE-176916-MS presented at the SPE Asia Pacific Unconventional Resources Conference and Exhibition, Brisbane, Australia.
- Vishkai M, Gates I (2019) On multistage hydraulic fracturing in tight gas reservoirs: montney Formation, Alberta, Canada. *J Petrol Sci Eng* 174:1127–1141
- Wang S, Chen Z, Chen S (2019) Applicability of deep neural networks on production forecasting in Bakken shale reservoirs. *J Petrol Sci Eng* 179:112–125
- Weng X, Kresse O, Chuprakov C, Prioul C, Ganguly R (2014) Applying complex fracture model and integrated workflow in unconventional reservoirs. *J Petrol Sci Eng* 124:468–483
- Wu K, Olson JE (2015) Simultaneous multifracture treatments: fully coupled fluid flow and fracture mechanics for horizontal wells. *SPE J* 20(02):337–346
- Wu Q, Liang X, Xian C, Li X (2015) Oil-to-production integration ensures effective and efficient south China Marine shale gas. *China Petroleum Explor* 20(4):1–23
- Yong R, Chang C, Zhang D, Wu J, Huang H, Jing D, Zheng J (2021) Optimization of shale-gas horizontal well spacing based on geology–engineering–economy integration: a case study of Well Block Ning 209 in the national shale gas development demonstration area. *Natural Gas Industry* 8(1):98–104
- Zhang H, Yang H, Yin G, Wang H, Xu K, Liu X, Wang Z (2020) Application practice of key technologies of geology-engineering integration for efficient development in the Kelasu structural belt. *Tarim Basin China Petroleum Explor* 25(2):120
- Zhao G, Yao Y, Wang L, Adenutsi CD, Feng D, Wu W (2022) Optimization design of horizontal well fracture stage placement in shale gas reservoirs based on an efficient variable-fidelity surrogate model and intelligent algorithm. *Energy Rep* 8:3589–3599
- Zillur R, Bartko K, Al-Qahtani MY (2002) Hydraulic fracturing case Histories in the carbonate and sandstone reservoirs of Khuff and Pre-Khuff formations, Ghawar Field, Saudi Arabia. Paper SPE-77677-MS presented at the SPE Annual Technical Conference and Exhibition, San Antonio, Texas, USA.

Publisher's Note Springer Nature remains neutral with regard to jurisdictional claims in published maps and institutional affiliations.